AIP | Applied Physics Letters

Carrier formation dynamics of a small-molecular organic photovoltaic

Takahiro Akaba, Kouhei Yonezawa, Hayato Kamioka, Takeshi Yasuda, Liyuan Han et al.

Citation: Appl. Phys. Lett. **102**, 133901 (2013); doi: 10.1063/1.4800532
View online: http://dx.doi.org/10.1063/1.4800532
View Table of Contents: http://apl.aip.org/resource/1/APPLAB/v102/i13
Published by the AIP Publishing LLC.

Carrier formation dynamics of a small-molecular organic photovoltaic

Takahiro Akaba,[1] Kouhei Yonezawa,[2] Hayato Kamioka,[1,2,3] Takeshi Yasuda,[4] Liyuan Han,[4] and Yutaka Moritomo[1,2,3,a)]

[1]*School of Science and Engineering, University of Tsukuba, Tsukuba 305-8577, Japan*
[2]*Graduate School of Science and Engineering, University of Tsukuba, Tsukuba 305-8577, Japan*
[3]*Tsukuba Research Center for Interdisciplinary Materials Science (TIMS), University of Tsukuba, Tsukuba 305-8577, Japan*
[4]*Photovoltaic Materials Unit, National Institute for Materials Science (NIMS), Tsukuba 305-0047, Japan*

(Received 18 December 2012; accepted 25 March 2013; published online 3 April 2013)

We investigated carrier formation dynamics in a small-molecular bulk heterojunction solar cell, 2,5-di-(2-ethylhexyl)-3,6-bis-(5″-*n*-hexy-[2,2′,5′,2″]terthiophen-5-yl)-pyrrolo[3,4-c]pyrrolo-1,4-dione/[6,6]-phenyl C_{71}-butyric acid methyl ester, with low bandgap ($E_{gap} \approx 1.5$ eV). The photoinduced absorption (PIA) spectra of the blend film were decomposed into three PIAs, i.e., those due to donor exciton (D^*), acceptor exciton (A^*), and mobile carrier (D^+). The analysis revealed carrier conversion from D^* with a conversion time of ~1.3 ps. © *2013 American Institute of Physics*. [http://dx.doi.org/10.1063/1.4800532]

Among numerous photovoltaic devices, bulk heterojunction (BHJ)[1,2] solar cells have attracted significant attention because a large area, highly efficient, and flexible photovoltaic device is expected by the role-to-role production process. The BHJ solar cells typically consist of an active layer, where the donor (D) phase is intimately intermixed with the acceptor (A) phase, a tin-doped indium oxide (ITO) anode, and an Al cathode. Reflecting the enlargement of the D/A interface area in the BHJ solar cell, the power conversion efficiency (PCE) reaches 9.2% (Ref. 3) with appropriate low bandgap donor polymer.[4] The donor phase of the active layer has been dominated by polymeric materials, because their film is easy-to-make and exhibits better morphology than their small-molecule counterparts. The polymers, however, suffer from synthetic reproducibility and difficult purification procedures, which may hinder commercial viability.

Small-molecular materials have the advantage of easiness of synthesis and purification. In addition, they have greater tendency to self-assemble into order domains, which leads to high carrier mobility. These properties make small-molecules promising class of donor materials for the BHJ solar cells. Among them, deketopyrrolopyrrole (DPP) pigments were developed in the early 1970s, and have been widely used in inks, paints, and plastics.[5] Recently, Nguyen's group reported that thiophene-based oligomers incorporating a DPP unit are excellent donor materials for the BHJ solar cells.[5–7] These materials exhibit intense absorption at long wavelengths and high field-effect mobility. They demonstrated solar cells with PECs of 3.0% using an oligothiophene-DPP molecule with ethylhexyl substituents [2,5-di-(2-ethylhexyl)-3,6-bis-(5″-*n*-hexy-[2,2′,5′,2″]terthiophen-5-yl)-pyrrolo[3,4-c]pyrrolo-1,4-dione (SMDPPEH): see Fig. 1] and [6,6]-phenyl C_{71}-butyric acid methyl ester ($PC_{70}BM$). The ethylhexyl groups make the donor material soluble (≥20 mg/ml in chloroform, chlorobenzene, or toluene) and thermally stable (m.p. = 160 °C).

In this letter, we investigated the carrier formation dynamics in SMDPPEH/$PC_{70}BM$ blend film by means of femtosecond time-resolved pump and probe spectroscopy. The power conversion processes in the BHJ solar cells involve (i) exciton formation and migration to the D/A interface, (ii) exciton dissociation into carriers (electron and hole), and (iii) slow carrier transport and collection at the electrodes. The time-resolved spectroscopy is a powerful tool to clarify the carrier formation dynamics [(i) and (ii)] in the subpicosecond region.[8–13] Careful decomposition analysis of the photoinduced absorption (PIA) spectra into those due to D^*, A^*, and D^+ revealed the carrier conversion from D^* with a conversion time of ~1.3 ps. The slow conversion time is ascribed to small band offset ($\Delta E = 0.2$ eV) of lowest

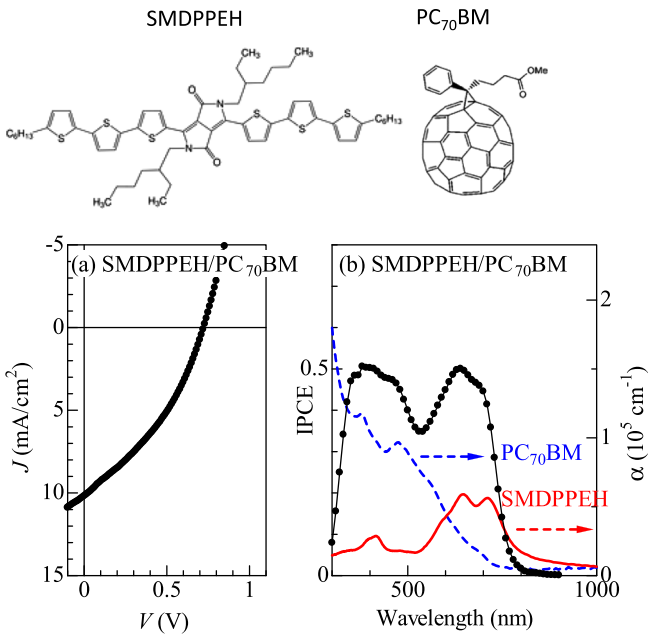

FIG. 1. (a) Current density (J)–voltage (V) curve of SMDPPEH/$PC_{70}BM$ BHJ solar cell. (b) IPCE spectrum of SMDPPEH/$PC_{70}BM$ BHJ solar cell (solid circles). Solid and broken curves are absorption coefficient (α) of SMDPPEH and $PC_{70}BM$ films, respectively.

a)E-mail: moritomo.yutaka.gf@u.tsukuba.ac.jp

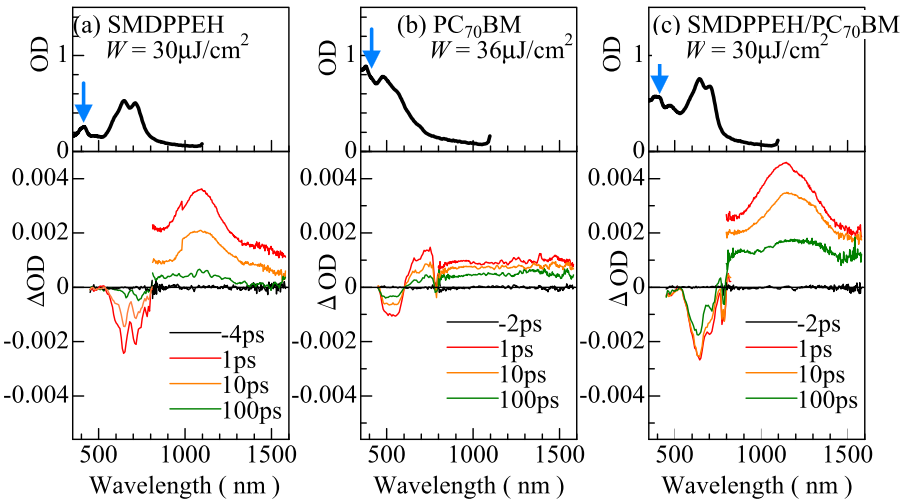

FIG. 2. Absorption (OD) spectra and differential absorption (ΔOD) spectra of (a) SMDPPEH, (b) $PC_{70}BM$, and (c) SMDPPEH/$PC_{70}BM$ films at 300 K. Excitation wavelength was 400 nm (downward arrows).

unoccupied molecular orbital (LUMO). The temporal evolution of the PIA due to D^+, however, implies a hidden $A^* \rightarrow D^+$ conversion process, whose conversion time is probably shorter than the time resolution ($\leq$0.2 ps) of the system.

We fabricated the SMDPPEH/$PC_{70}BM$ solar cell in the following configuration: ITO/poly(3,4-ethylenedioxythiophene) (PEDOT): poly(styrenesulfonate) (PSS) (40 nm)/active layer (52 nm)/LiF (1 nm)/Al (80 nm). SMDPPEH was purchased from Sigma-Aldrich and used as received. A thin layer (40 nm) of PEDOT: PSS was spin-coated onto the ITO and dried at 110 °C for 10 min on a hot plate in air. The substrate was then transferred to an N_2 glove box and dried again at 110 °C for 10 min on a hot plate. An chlorobenzene solution of SMDPPEH: $PC_{70}BM$ with a ratio of 1:1 by weight is subsequently spin-coated onto the PEDOT: PSS surface to form the active layer. Finally, LiF (1 nm) and Al (80 nm) were deposited onto the active layer by conventional thermal evaporation at a chamber pressure lower than 5×10^{-4} Pa, which provided the devices with an active area of 2×2 mm^2.

For the time-resolved spectroscopy, the SMDPPEH/$PC_{70}BM$ blend film was spin-coated on quartz substrates, and was dried in an inert N_2 atmosphere. For comparison, we prepared spin-coated SMDPPEH ($PC_{70}BM$) film on quartz substrates from chlorobenzene (chloroform) solution. The thicknesses of the SMDPPEH, $PC_{70}BM$, and SMDPPEH/$PC_{70}BM$ blend films were 39, 50, and 96 nm, respectively. The time-resolved spectroscopy was carried out in a pump-probe configuration at room temperature, details of which were described in the literature.[13] Spot sizes of the pump and probe pulses were 5 and 3 mm in diameter, respectively. The differential absorption spectra (ΔOD) are expressed as $\Delta OD \equiv -\log(\frac{I_{on}}{I_{off}})$, where I_{on} and I_{off} are the transmitted light intensity with and without pump excitations, respectively. The time resolution of the system is ~0.2 ps.

Figure 1(a) shows current density-voltage (J–V) curve of the solar cell. The curve was measured using an ADCMT 6244 DC voltage current source/monitor under AM 1.5 solar-simulated light irradiation of 100 mW cm^{-2} (OTENTO-SUN III, Bunkou-keiki Co., Ltd.). The cell exhibits a open circuit voltage (V_{oc}) of 0.72 V, a short circuit current (J_{sc}) of 10.19 mA cm^{-2}, a fill factor (F.F.) of 0.36, and a PCE (E_{ff}) of 2.62%. Figure 1(b) shows incident photon to current conversion efficiency (IPCE) spectrum of the cell, which was measured using a SM-250 system (Bunkou-keiki Co., Ltd.). The magnitude of IPCE [Fig. 1(b)] is 40%-50% in the wavelength region of 350-700 nm.

Figure 2 shows ΔOD spectra of (a) SMDPPEH, (b) $PC_{70}BM$, and (c) SMDPPEH/$PC_{70}BM$ films. In all the films, the ΔOD spectra consist of negative signals in the short-wavelength region and positive signals in the long-wavelength region. The negative signals at ≈600 nm in the neat SMDPPEH and SMDPPEH/$PC_{70}BM$ blend films are ascribed to the ground state bleach (GSB) of SMDPPEH, while that at ≈550 nm in the neat $PC_{70}BM$ film is ascribed to the GSB of $PC_{70}BM$. In the neat SMDPPEH film [Fig. 2(a)], the broad positive signal at ~1100 nm is ascribed to the PIA due to D^*. In the neat $PC_{70}BM$ film [Fig. 2(b)], the broad positive signal extending above 600 nm is ascribed to the PIA due to A^*. In the SMDPPEH/$PC_{70}BM$ blend film [Fig. 2(c)], the broad positive signal in the infrared region exhibits a characteristic red-shift from ~1100 nm at 1 ps to ~1200 nm at 10 ps. We confirmed that the spectral profile becomes independent of the delay time (t) for $t \geq 2$ ps. So, we ascribed the broad positive signal ($t \geq 2$ ps) to the PIA due to D^+.

Now, let us decompose the PIA spectra (ϕ_{exp}) of the blend film into those due to D^*, A^*, and D^+ as

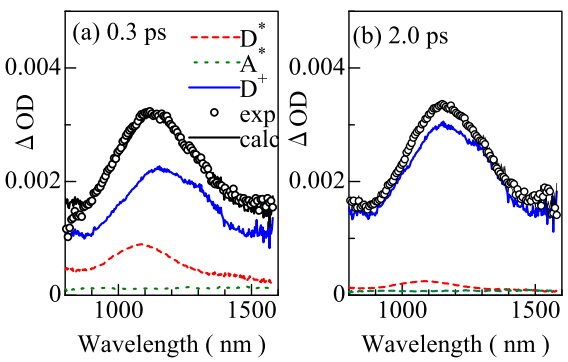

FIG. 3. Decomposition of the ΔOD spectra of SMDPPEH/$PC_{70}BM$ film into PIAs due to D^*, A^*, and D^+: (a) at 0.3 ps and (b) at 2.0 ps. Open circles represent the experimental data, while thin solid curve is the calculation. The broken, dotted, and solid curves are the PIAs due to D^*, A^*, and D^+, respectively.

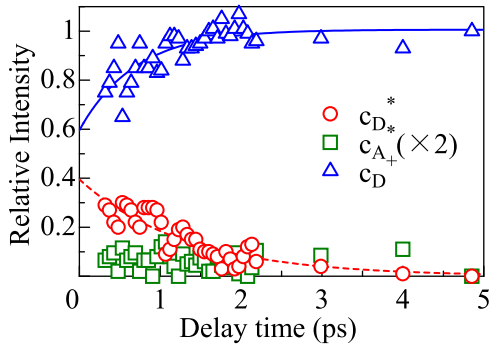

FIG. 4. Delay time dependence of the spectral weights, c_{D^*}, c_{A^*}, and c_{D^+}, in SMDPPEH/$PC_{70}BM$ film. Excitation wavelength was 400 nm. Solid curve is result of the least-squares fitting with $A \cdot (1 - e^{-\frac{t}{\tau_{rise}}}) + C_0$. Broken curve is result of the least-squares fitting with $A \cdot e^{-\frac{t}{\tau_{decay}}}$.

$$\phi_{cal} = c_{D^*} \cdot \phi_{D^*} + c_{A^*} \cdot \phi_{A^*} + c_{D^+} \cdot \phi_{D^+}, \quad (1)$$

where c_{D^*}, c_{A^*}, and c_{D^+} are the spectral weights and ϕ_{D^*}, ϕ_{A^*}, and ϕ_{D^+} are the PIAs due to D^*, A^*, and D^+. We regarded the PIAs of SMDPPEH (at 2 ps), $PC_{70}BM$ (1 ps), and SMDPPEH/$PC_{70}BM$ (5 ps) films as ϕ_{D^*}, ϕ_{A^*}, and ϕ_{D^+}, respectively. We performed least-squares fitting of ϕ_{exp} with ϕ_{cal} with three adjustable parameters, i.e., c_{D^*}, c_{A^*}, and c_{D^+}. We searched the best parameter set within the $150 \times 150 \times 150$ parameter space: $c_{D^*} = 0.00, 0.01, \ldots, 1.50$, $c_{A^*} = 0.00, 0.01, \ldots, 1.50$, and $c_{D^+} = 0.00, 0.01, \ldots, 1.50$. Figure 3 shows prototypical examples of the decomposition.

Thus, the obtained spectral weights are plotted in Fig. 4 against t. Among the parameters, c_{D^+} and c_{D^*} exhibit significant time dependence. The intensity (open circles) of c_{D^*} gradually decreases with time, and disappears above ~3 ps. The decay time (τ_{decay}) of c_{D^*} is estimated to be ~1.3 ps (broken curves in Fig. 4). The magnitude of τ_{decay} (~1.3 ps) is much slower as compared with that ($\tau_{decay} \leq 0.5$ ps (Ref. 14)) in PTB1/$PC_{70}BM$ blend film. On the other hand, the intensity (open triangle) of c_{D^+} gradually increases with time. The extrapolation of the $c_{D^+} - t$ curve appears to intersect the vertical axis at finite value. Therefore, we performed a least-squares fitting with constant term: $A \cdot (1 - e^{-\frac{t}{\tau_{rise}}}) + C_0$. The rise time ($\tau_{rise}$) of c_{D^+} is estimated to be ~0.7 ps, which is much faster than τ_{decay} (~1.3 ps) of c_{D^*}. This observation, together with the constant term ($C_0 = 0.6$), suggests a faster carrier formation process in addition to the $D^* \rightarrow D^+$ process. Judging from the fact that the photo-excitation at 400 nm creates considerable A^* in the A phase [see Fig. 2(b)], the hidden process is probably the $A^* \rightarrow D^+$ process. Actually, such a process is observed in low-band gap PTB7/$PC_{70}BM$ blend film.[12]

TABLE I. Amplitudes (A and C) and relaxation time (τ) of PIAs and GSBs in SMDPPEH, $PC_{70}BM$, and SMDPPEH/$PC_{70}BM$ blend films. The parameters were obtained by least-squares fitting with $\Delta OD = A \cdot e^{-\frac{t}{\tau}} + C$.

	SMDPPEH		$PC_{70}BM$		Blend	
	GSB	PIA	GSB	PIA	GSB	PIA
A ($\times 10^{-3}$)	−0.90	1.68	−0.44	0.63	−1.09	1.75
τ (ps)	79	52	149	151	106	117
C ($\times 10^{-3}$)	−0.17	0.20	−0.19	0.19	−1.36	0.72

Let us investigate the slow decay dynamics of the photogenerated particles, i.e., D^*, A^*, and D^+. Figure 5 shows temporal evolutions of the GSB and PIA signals in (a) SMDPPEH, (b) $PC_{70}BM$, and (c) SMDPPEH/$PC_{70}BM$ films. Solid curves are results of least-squares fitting with an exponential function, $\Delta OD = A \cdot e^{-\frac{t}{\tau}} + C$. The obtained parameters are listed in Table I. In the neat SMDPPEH film, the lifetime (≈52 ps) of D^* is nearly the same as that of the GSB signal. The lifetime (≈52 ps) of D^* is significantly longer than those in regioregular-P3HT (8 ps (Ref. 8)) and in F8T2 (2.7 ps (Ref. 11)). We note that the lifetime (≈150 ps) of A^* is also long in the neat $PC_{70}BM$ film. These long lifetimes of D^* and A^* suggest that their decays are governed by the radiative recombination, not by the nonradiative channel. The decay times of D^* ($\tau_{decay} \sim 1.3$ ps) of the blend film are two-order faster than those in the neat film. The fast decay time is ascribed to the exciton dissociation process into the carriers. The PIA signal of the blend film exhibits a large constant component (C), which is ascribed to the long-lived carriers.

Let us discuss the interrelation between carrier formation dynamics and the band offset (ΔE) of LUMO and highest unoccupied molecular orbital (HOMO). In the conventional $D^* \rightarrow D^+$ process, an electron on donor HOMO transfers to acceptor LUMO at the D/A interface. Then, ΔE of LUMO is considered to be the dominative parameter for the carrier conversion process. On the other hand, a hole (an electron) state is photocreated at the acceptor HOMO (LUMO) in the $A^* \rightarrow D^+$ process. After

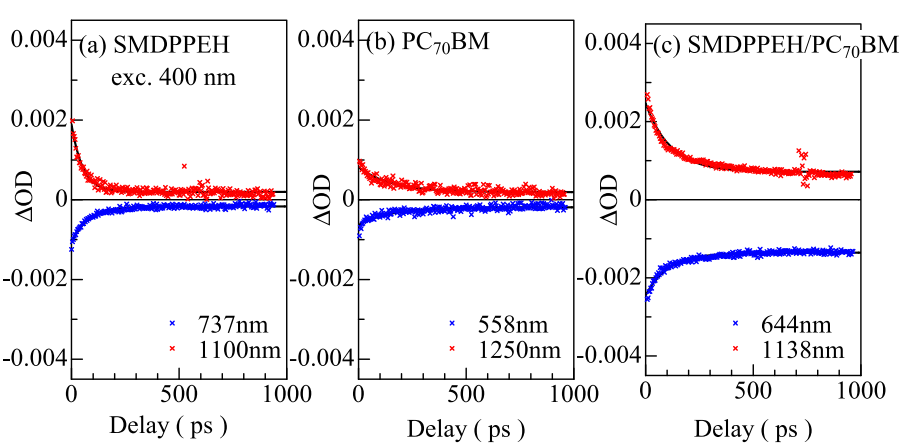

FIG. 5. Temporal evolutions of GSB and PIA signals in (a) SMDPPEH, (b) $PC_{70}BM$, and (c) SMDPPEH/$PC_{70}BM$ films. Excitation wavelength was 400 nm. Solid curves are results of least-squares fitting with an exponential function, $\Delta OD = A \cdot e^{-\frac{t}{\tau}} + C$.

that, an electron on donor HOMO transfers to acceptor HOMO. In this case, ΔE of HOMO is the dominative parameter for the carrier conversion process. In SMDPPEH/$PC_{70}BM$,[7] the magnitude of $\Delta E(=0.2\,\mathrm{eV})$ of LUMO is much smaller than that (=0.8 eV) of HOMO. The small ΔE of LUMO is responsible for the slow carrier conversion time ($\tau_{decay} \sim 1.3$ ps) from D^*. The large ΔE of HOMO implies a faster carrier conversion process from A^*, which is discernible as the constant term of the PIA due to D^+ (see Fig. 4).

Recently, Ohkita's group[15] proposed a hole transfer from donor polymer to [6,6]-phenyl C_{61}-butyric acid methyl ester (PCBM) on a time scale of nanoseconds. The hole transfer scenario well explains the commonly observed enhancement of hole transport in polymer/PCBM blend.[16] The mobile carriers (D^+), which are photocreated on a time scale of picoseconds, reach the collecting electrode via the hopping process within the donor domain and/or the hole transfer into the acceptor molecule.

In summary, we investigated the carrier formation dynamics in SMDPPEH/$PC_{70}BM$ blend film by means of femtosecond time-resolved pump and probe spectroscopy. Careful decomposition analysis of the PIA spectra into those due to D^*, A^*, and D^+ revealed $D^* \rightarrow D^+$ conversion process with conversion time of ~1.3 ps. The temporal evolution of the PIA due to D^+ implies a hidden $A^* \rightarrow D^+$ conversion process.

This work was supported by a Grant-in-Aid for Young Scientists (B) (22750176) for Scientific Research from the Ministry of Education, Culture, Sports, Science, and Technology, Japan.

[1]M. Hiramoto, H. Fujiwara, and M. Yokoyama, Appl. Phys. Lett. **58**, 1062 (1991).
[2]N. S. Sariciftci, L. Samilowitz, A. J. Heeger, and F. Wudl, Science **258**, 1474 (1992).
[3]Z. He, C. Zhong, S. Su, M. Xu, H. Wu, and Y. Cao, Nature Photon. **6**, 593 (2012).
[4]Y. Liang, Y. Wu, D. Feng, S.-T. Tsai, H.-J. Son, G. Li, and L. Yu, J. Am. Chem. Soc. **131**, 56 (2009).
[5]S. Qu and H. Tian, Chem. Commun. **48**, 3039 (2012).
[6]A. B. Tamayo, B. Walker, and T.-Q. Nguyen, J. Phys. Chem. C **112**, 11545 (2008).
[7]A. B. Tamayo, X.-D. Dang, B. Walker, J. Seo, T. Kent, and T.-Q. Nguyen, Appl. Phys. Lett. **94**, 103301 (2009).
[8]I.-W. Hwang, D. Moses, and A. J. Heeger, J. Phys. Chem. C **112**, 4350 (2008).
[9]J. Guo, H. Ohkita, H. Benten, and S. Ito, J. Am. Chem. Soc. **132**, 6154 (2010).
[10]R. A. Marsh, J. M. Hodgkiss, S. Albert-Seifried, and R. H. Friend, Nano Lett. **10**, 923 (2010).
[11]K. Yonezawa, M. Ito, H. Kamioka, T. Yasuda, L. Han, and Y. Moritomo, Appl. Phys. Express **4**, 122601 (2011).
[12]K. Yonezawa, H. Kamioka, T. Yasuda, L. Han, and Y. Moritomo, Appl. Phys. Express **5**, 042302 (2012).
[13]K. Yonezawa, M. Ito, H. Kamioka, T. Yasuda, L. Han, and Y. Moritomo, Adv. Opt. Technol. **2012**, 316045.
[14]J. Guo, Y. Liang, J. Szarko, B. Lee, H.-J. Son, B. S. Rolczynski, L. Yu, and L. X. Chen, J. Phys. Chem. B **114**, 742 (2010).
[15]S. Yamamoto, H. Ohkita, H. Benten, and S. Ito, Adv. Funct. Mater. **22**, 3075 (2012).
[16]A. Gadisa, K. Tvingstede, K. Vandewal, F. Zhang, J. V. Manca, and O. Lnganäs, Adv. Mater. **22**, 1008 (2010).